Computer simulations of cathodeless, high-brightness electron-beam production by multiple laser beams in plasmas

R. G. Hemker, K.-C. Tzeng, W. B. Mori, and C. E. Clayton
Department of Physics and Astronomy, University of California at Los Angeles, Los Angeles, California 90095-1547

T. Katsouleas
Department of Electrical Engineering, University of Southern California, Los Angeles, California 90089-0271
(Received 15 July 1997)

The use of two crossed laser pulses in a plasma for the cathodeless production of high-current low-emittance electron beams [D. Umstadter, J. K. Kim, and E. Dodd, Phys. Rev. Lett. **76**, 2073 (1996)] is examined with fully relativistic, two-and-a-half-dimensional particle-in-cell simulations. Estimates for the number of injected particles, their energy spread, and their emittance are given as functions of the amplitude and timing of the injection pulse relative to the drive pulse of the laser wake field accelerator. The physical mechanism of the trapping of particles is examined based on single particle phase space trajectories in the simulations and numerical calculations. [S1063-651X(98)08405-0]

PACS number(s): 52.40.Nk, 41.75.Lx, 52.65.Rr

INTRODUCTION

Recently Umstadter, Kim, and Dodd [1] proposed the use of two orthogonal laser pulses in a plasma to trap and accelerate an ultrashort bunch of electrons. As envisioned, the first (or drive) pulse creates a plasma wave which is below its self-trapping or wave-breaking threshold. The transverse ponderomotive force of the second (or injection) pulse was argued to give electrons an extra kick forward in the wake direction, enabling them to be trapped and accelerated in the wake of the drive pulse. This geometry is illustrated in Fig. 1. Such a cathodeless injector (or perhaps more correctly, a plasma cathode) is of interest for a wide variety of applications including an injector for future linear accelerator technologies with short wavelength accelerating structures, a source of short pulses of light or x rays, or a source of electron bursts for pulsed radiology and ultrafast pump-probe chemistry [2]. For plasma accelerator applications in particular, the scheme naturally overcomes problems of synchronizing the injector with the accelerator. Moreover, the rapid acceleration of the bunch in the plasma (order of 10–100 GeV/m) [3–6] minimizes the effect of space charge that would be severe for such dense beams (10^{14}–10^{18} cm^{-3}) produced from a conventional thermionic photocathode [7].

The original analysis of Ref. [1] used single particle theory and estimates based on one-dimensional (1D) particle-in-cell (PIC) simulations. In this paper, we present results from a detailed 2D PIC simulation analysis of this concept. We find that our results support the feasibility of such a cathodeless injection scheme, but that in the regime studied here the physical mechanism for the trapping is different from the one originally suggested. Furthermore, we show that the number of particles, the emittance, and the energy spread can all depend sensitively on the laser parameters and the injection phase. Depending on the applications, these results place constraints on the allowable shot to shot jitter of the injection laser. Finally based on insight into the trapping mechanism, we put forth additional geometries, e.g., copropagating and counterpropagating pulses, as well as related injection schemes.

REVIEW OF PARTICLE DYNAMICS

We next briefly review the dynamics of electrons in relativistic plasma waves because the paper bridges two fields, beam and plasma physics. Consider an electron being accelerated in a plasma wave of the form

$$\phi = \phi_0(1 - x_2^2/w_p^2)\sin[k_p(x_1 - \nu_\phi t)], \tag{1}$$

where ν_ϕ is the phase velocity of the wave, and w_p is a parameter describing the width of the plasma wave. This potential describes the behavior of particles close to the center of a typical plasma wave. We assume $\nu_\phi \cong c$, i.e., relativistic plasma waves. The subscripts 1 and 2 refer to direc-

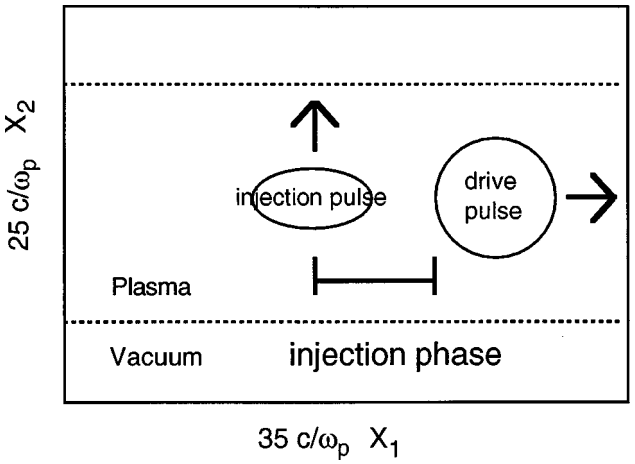

FIG. 1. Geometry of the cathodeless injector concept [1]. The injection phase of the injection pulse is defined by the distance between the trailing edge of the drive pulse and the center of the injection pulse when it crosses the drive pulse.

tions parallel and perpendicular, respectively, to the plasma wave's direction of propagation. The equations of motion for an individual electron are

$$\frac{d}{dt}\,p_1 = -eE_1 = e\phi_0 k_p (1-x_2^2/w_p^2)\cos[k_p(x_1-\nu_\phi t)], \tag{2}$$

$$\frac{d}{dt}\,p_2 = -eE_2 = -2e\phi_0\,\frac{x_2}{w_p^2}\,\sin[k_p(x_1-\nu_\phi t)]. \tag{3}$$

The acceleration of single electrons in these fields has been studied extensively [8–10]. An injected electron accelerated along the axis, $x_1=0$, will be trapped if its injection energy (the initial kinetic energy) exceeds the trapping threshold [8,10,11]

$$W_i \approx mc^2(\gamma_\phi^2\{\overline{\phi_0}+1/\gamma_\phi-\beta_\phi[(\overline{\phi_0}+2/\gamma_\phi)\overline{\phi_0}]^{1/2}\}-1)$$
$$\text{with}\quad \overline{\phi_0}=e\phi_0/(mc^2), \tag{4}$$

which reduces to $\frac{1}{2}[\overline{\phi_0}+(1/\overline{\phi_0})]-1$ as $\gamma_\phi\to\infty$.

Once trapped, an electron is accelerated, and its speed eventually exceeds the phase velocity of the wave. The acceleration process ceases after the electron outruns the wave and encounters decelerating forces. If $x_2=0$, then the maximum energy gain is [3,8,10,11]

$$W_f - W_i \equiv \Delta W \cong 2\gamma_\phi[1+\eta\overline{\phi_0}\gamma_\phi]mc^2, \tag{5}$$

where η is 2 if the particle slips through a full π phase of the accelerating bucket. ΔW is approximately $2\eta\phi_0\gamma_\phi^2 mc^2$ if $\overline{\phi_0}\gamma_\phi \gg 1$. The dephasing distance can be estimated by calculating the distance it takes for the electron moving at the speed of light, c, to move forward a half wavelength in a wave moving at $\nu_\phi \cong c$. This gives [8,10,11]

$$L_{\rm dp} = \tfrac{1}{2}\eta\gamma_\phi^2\lambda_p = \eta\pi\gamma_\phi^2 c/\omega_p\,. \tag{6}$$

An electron which is not on the axis, $x_2\neq 0$, will also experience transverse, i.e., defocusing or focusing fields, as given by Eq. (3). Electrons in the defocusing phase of the wave accelerate away from the axis, and are eventually lost [8–10]. Electrons in the focusing phase execute betatron oscillations (in x_2) as they accelerate along x_1, so only electrons which reside in both focusing and accelerating fields are accelerated to the dephasing limit [8–10]. These fields are $\pi/2$ out of phase, and therefore only a quarter of a plasma wave wavelength can be used for acceleration. This reduces the maximum energy gain and the dephasing length given above by roughly a factor of 2 [i.e., $\eta=1$ in Eq. (5)]. In finite-width plasma waves, additional second order focusing terms may extend the range of phases which have both focusing and accelerating forces [12,13].

An accelerated beam is characterized by its energy and normalized emittance ε_n where ε_n is a measure of the area of the beam in transverse phase space. Note that Eq. (3) has the adiabatic invariant p_2x_2 for each individual particle. For a relativistic beam (i.e., $\gamma\gg 1$), this area is given by the product of the beam's transverse spot size σ, angular divergence $\theta=p_2/p_1$, and energy, $\gamma\cong p_1/mc$; therefore $\varepsilon_n=\pi\gamma\theta\sigma$, and it is conserved under ideal conditions. The evolution of the beam's spot size is described by the envelope equation [14]

$$\frac{d^2}{dx_1^2}\,\sigma+\frac{1}{\gamma}\frac{d\gamma}{dx_1}\frac{d\sigma}{dx_1}-\left(\frac{\varepsilon_n}{\pi}\right)^2\frac{1}{\gamma^2\sigma^3}\left[1+\frac{2\pi^2}{\gamma}\left(\frac{\sigma}{\varepsilon_n}\right)^2\frac{1}{I_A}-\frac{\gamma\omega_B^2\sigma^4}{c^2}\left(\frac{\pi}{\varepsilon_n}\right)^2\right]=0, \tag{7}$$

where I is the beam's current, $I_A\cong mc^3/e$, is the Alfven current, σ_0 is the initial spot size, and $\omega_B^2=2|\overline{\phi_0}|c^2/w_p^2$ is the betatron frequency for the potential given by Eq. (1). The first term in the large square bracket is due to diffraction, the second term is due to self-space-charge, and the third term is due to the external focusing forces (i.e., of the plasma wave), respectively.

The parameter characterizing the ratio of the space charge term to the diffraction term in the beam envelope equation is given by

$$\rho=\frac{2\pi^2}{\gamma}\left(\frac{\sigma^2}{\varepsilon_n^2}\right)\frac{I}{I_A}. \tag{8}$$

If the effects of space charge can be neglected, then the equilibrium state of a matched beam (σ does not change during the acceleration) can be obtained by balancing the two remaining force terms. These two terms are the one arising from the diffraction, and the transverse external force term. The external force term can be related to the amplitude E_{10} of the accelerating electric field of the plasma wave, which is a quantity we observe in our simulations, i.e., $\phi_0=-E_{10}/k_p$. The resulting condition for a matched beam is

$$\frac{1}{4\pi^2\gamma}\,\frac{mc\omega_p}{eE_{10}}\left(\frac{\varepsilon_n}{\sigma}\right)^2\left(\frac{w_L}{\sigma}\right)^2=1. \tag{9}$$

Here we also replace w_p with $w_L/\sqrt{2}$, where w_L is the laser spot size because the transverse profile of the longitudinal field of the plasma wave is proportional to the transverse profile of the laser intensity $E_{10}\propto E_L^2$, since the ponderomotive force of the laser pulse causes the plasma wake [9,15]. If the expression on the left side of the equation is larger than unity, the focusing forces dominate the diffraction.

An estimate of the upper limit of the emittance of a beam in cathodeless injection schemes can be found from the acceptance [16] of the plasma wave. The acceptance is the transverse phase space volume that can be accelerated by the system. For a plasma wave the acceptance can be approximately calculated by assuming a transverse potential profile that is responsible for the focusing forces of the plasma wave. For a given transverse potential, $\phi_2\equiv\phi_0(1-x_2^2/w_p^2)$, we can find the maximum transverse momentum p_2 that a particle can have at a given transverse position x_2 before the particle can escape the potential well. Since the plasma wave as well as the particle both move with almost the same velocity c, the potential function ϕ_2 will change slowly, and we will neglect that change here.

We start with the condition that an electron is trapped transversely in the plasma wave's potential well, i.e., that the transverse kinetic energy has to be smaller than the energy needed to escape the transverse potential $|E_{k,2}|<|E_{p,2}|$,

$$\sqrt{p_2^2c^2+p_1^2c^2+m^2c^4}-\sqrt{p_1^2c^2+m^2c^4}<-e\phi_2 \quad (\phi_2\leqslant 0).$$

This can be solved, giving an inequality for the p_2 of a trapped electron:

$$|p_2|c<\sqrt{(-e\phi_2+\sqrt{p_1^2c^2+m^2c^4})^2-m^2c^4-p_1^2c^2}.$$

Rearranging terms gives the following result:

$$|p_2|<mc\left(-\frac{2e\phi_2\gamma_1}{mc^2}\right)^{1/2}\left(1+\frac{-e\phi_2}{2mc^2}\frac{1}{\gamma_1}\right)^{1/2}\equiv p_{2,\max}(x_2), \tag{10}$$

where $\gamma_1^2=1+(p_1/mc)^2$.

For linear waves $\phi_2=e\phi_2/(mc^2)\leqslant 1/2$; so to lowest order the second square root term can be approximated as unity. We use Eq. (10) to calculate the normalized acceptance [16]

$$A_n=2\int_{-\infty}^{\infty}\frac{p_{2,\max}}{mc}\,dx_2=2\int_{-\infty}^{\infty}\frac{\sqrt{-2me\phi_2\gamma_1}}{mc}\,dx_2. \tag{11}$$

Assuming the potential given in Eq. (1), and replacing w_p with $w_L/\sqrt{2}$, we obtain an approximate result for A_n by replacing the integration limits with $w_L/\sqrt{2}$ and $-w_L/\sqrt{2}$:

$$A_n=2\sqrt{2me\phi_0\cos(\alpha)\gamma_1}\,\frac{1}{mc}\int_{-w_L/\sqrt{2}}^{w_L/\sqrt{2}}\left(1-2\frac{x_2^2}{w_L^2}\right)^{1/2}dx_2$$

$$=2\pi w_L\sqrt{\gamma_1\phi_0}\sqrt{\cos(\alpha)}, \tag{12}$$

where α is the phase of the electron in the wave with respect to the potential maximum. If we assume γ_1 is of the order of the trapping threshold, then $\phi_0\gamma_1=O(1)$, so ε_n for any cathodeless injection scheme is bounded by $\varepsilon_n<2w_L\pi$. If the trapping of a particle bunch by a plasma wave does not take place at the maximum of the potential, then $\cos(\alpha)$ is smaller than 1 and the emittance of the beam can be expected to be smaller than this upper bound. Note that if Eq. (9) is solved for ε_n, then it results in $\varepsilon_n=2\pi\sqrt{\gamma eE_{10}/(mc\omega_p)}(\sigma/w_L)^2\sigma$. Using $\gamma\approx\gamma_1$, $\phi_0=ek_p^{-1}E_{10}/(mc^2)$, and $\sigma=w_L$ leads to $\varepsilon_n=2\pi w_L\sqrt{\gamma_1\phi_0}$. This means that the acceptance is the emittance for a matched beam.

SIMULATION RESULTS

The simulations are conducted with the single node version of the fully relativistic two-and-a-half-dimensional PIC code PEGASUS [17]. This code uses a simulation box which moves with the speed of light, and can therefore follow the laser pulse for extended periods of time. Even though the simulation box moves, all calculations are done in the rest frame of the plasma. PEGASUS uses the charge conserving algorithm in ISIS, and solves locally for E and B fields. Figure 1 shows the basic setup of the simulations. The following parameters are valid for most of the simulations results presented below, unless stated differently. The simulation box has a size of $35c/\omega_p$ in the x_1 direction, and $25c/\omega_p$ in the x_2 direction, and the simulations run for a time of $105\omega_p^{-1}$. The simulations use a 700×500 grid, a time step $dt=0.035\omega_p^{-1}$, and four particles per cell.

As the drive pulse starts to move in the x_1 direction into the cold plasma, it creates a plasma wave in its wake. This is due to the ponderomotive force of the drive pulse and it is the basis for the laser wake field accelerator (LWFA) [3,6,15]. At a later time the injection pulse is launched in a vacuum region at the side of the box and propagates in the x_2 direction, crossing the path of the drive pulse. The frequency ratio ω_0/ω_p between the laser frequency and the plasma frequency is 5 for both pulses, and both have their polarization in the plane of the simulation. (This means the drive pulse has mainly an E_2 component and the injection pulse mainly an E_1 component.) We adopt the notation in Ref. [1], where the normalized vector potential for the drive pulse is $a\equiv eA_y/mc^2=1$, and for the injection pulse is $b\equiv eA_x/mc^2=2$, unless stated otherwise. We observed in the simulation that the plasma wave amplitude caused by $a=1$ is about $\phi_0=0.45$. The transverse profile for each laser is given by a Gaussian with a spot size of $3c/\omega_p$. The temporal profile has a symmetric rise and fall of the form $f(x)=10x^3-15x^4+6x^5$ with $0\leqslant x=\tau/\tau_L\leqslant 1$. The value of τ_L is $\pi c/\omega_p$ for the drive pulse and $\frac{1}{2}\pi c/\omega_p$ for the injection pulse; thus the simulations have fewer laser cycles than in typical experiments. We define the injection phase ψ to be the distance between the back of the drive pulse and the center of the injection pulse as it crosses the axis. This is shown in Fig. 1.

In order to convert the simulation results to physical units, we assume a plasma density of 10^{16} cm^{-3}. If not stated differently, all quantities are given in normalized Gaussian units with the plasma frequency equal to 1. The number of accelerated electrons is estimated from the simulations as follows:

$$N=\frac{\text{Number of trapped simulation particles}}{\text{Number of particles per cell}}\times ndx_1dx_2\Delta x_3[(mc^2)/(4\pi e^2n)]^{3/2}. \tag{13}$$

Here n is the electron density in cm^{-3}, dx_1 and dx_2 are the cell sizes in the x_1 and x_2 directions, and Δx_3 is an assumed extension in the x_3 direction, dx_1, dx_2, and Δx_3 are in normalized units. We assume Δx_3 to be equal to Δx_2, the width of the group of accelerated particles in x_2, which assumes cylindrical symmetry for the accelerated beam. The normalized emittance is calculated as

$$\varepsilon_n=\gamma\frac{\Delta p_2}{p_1}\Delta x_2[(mc^2)/(4\pi e^2n)]^{1/2} \quad \text{with} \quad \gamma=\sqrt{p^2+1}\approx p_1. \tag{14}$$

Here p_1 is the average longitudinal momentum, and Δp_2 and Δx_2 are the width of the distributions of p_2 and x_2 for the group of accelerated particles. It should be noted that the number of electrons as well as the normalized emittance both scale with $n^{-1/2}$. All quantities, including the energy spread, are calculated after the final time step of the calculation, i.e., after a propagation distance of $105c/\omega_p$ [particles are trapped, $\gamma>\gamma_\phi$, between 50 and $60c/\omega_p$—see Fig. 4(a)]. The values of Δx_2 and Δp_2 are defined to be the standard deviations of the particle bunches for these quantities. The

energies of the trapped particles are around 10 MeV, which is of the order of the theoretical energy gain $\Delta W = 16$ MeV [Eq. (5), with $\eta = 1$, $\bar{\phi}_0 = 0.45$, and $\gamma_\phi = 5$] that would be obtained over the dephasing distance of $80c/\omega_p$ [Eq. (6)]. The trapping threshold for these simulations is 0.05 MeV [Eq. (4)]. The simulations show that trapped particles start close to the maximum accelerating gradient, which is consistent with the result above.

The engineering results of the simulations are summarized in Fig. 2. In Fig. 2(a), we plot the number of trapped electrons, the emittance, and the energy spread as a function of the injection phase for a fixed value of the injection amplitude, $b = 2.0$. In Fig. 2(b), we plot the same quantities as in Fig. 2(a), but as a function of the injection amplitude for a fixed value of the injection phase, $\psi = 1.3\pi$. All other parameters have the values given before. Note that negative values for ψ mean that the center of the injection pulse crosses the x_2 axis before the end of the drive pulse.

The most notable feature of Fig. 2(a) is the large variation of the three beam quantities as a function of ψ, and especially the strong difference in the number of particles and their emittance between positive injection phases larger and smaller than π. The direct overlap of the injection pulse with the drive pulse (i.e., an injection phase smaller than π) clearly yields the largest number of trapped particles. The maximum number of trapped electrons corresponds to 8×10^8 at a plasma density of 10^{16} cm^{-3} (or to 6×10^7 at a density of 10^{19} cm^{-3}). Note that 100% beamloading [18] corresponds to $N = 5 \times 10^5 \bar{\phi}_0 \sqrt{n_0 c m^3}$ A cm$^{-2} \approx 8 \times 10^9$ for $n_0 = 10^{16}$ cm^{-3}, where we use a laser beam cross section of $A = \pi w_p^2$ with $w_p = w_L/\sqrt{2} = (3/\sqrt{2})c/\omega_p$. Therefore, there is $\leq 10\%$ beamloading for negative and $\leq 1\%$ positive injection phases.

The number of particles decreases by an order of magnitude for injection phases larger than π. The normalized emittance, on the other hand, is better for injection phases larger than π, with the smallest normalized value of 3π mm mrad in a 10^{16}-cm^{-3} density plasma (or 0.1 π mm mrad at 10^{19} cm^{-3}). Note, from Eq. (12), that the acceptance for the plasma wave places an upper bound on the emittance of $2w_L\pi = 300\pi$ mm mrad for $n_0 = 10^{16}$ cm^{-3}. However, since the particles are trapped at a phase close to the maximum accelerating phase of the plasma wave (i.e., close to a zero for the focusing field), the cos term in Eq. (12) is small. We therefore expect the emittance to be smaller than this upper limit. For injection phases smaller than π, the emittance increases by a factor of 5. The emittance therefore seems to grow with the number of particles. Although this is suggestive of some sort of space charge degradation, we will show later that space charge is not important. Instead, we believe that the relatively larger emittance and number of particles at smaller ψ are both due to a stochastic interaction between the plasma and the overlapping laser fields.

The energy spread of the accelerated bunch also varies widely; it is between 2% and 17% at a beam energy of 10 MeV, and we expect the energy spread $\Delta E/E$ to scale as $1/\gamma$ for simulations with larger dephasing energies (i.e., larger values of ω_0/ω_p), since $\Delta E/E \propto \Delta E/\gamma$, and ΔE is not expected to change significantly. There is an interesting difference between the behavior of the energy spread and the number of particles on the one hand, and on the emittance on the other hand, for the larger injection phases in Fig. 2(a). The energy spread, and to some extent the number of particles, fluctuate as a function of ψ. The emittance remains almost constant which suggests that it is determined by qualities of the accelerating plasma wave and not by details of the injection process like the injection phase.

Although the simulations with $b = 2.0$ produce similar numbers of particles at $\psi = 1.3\pi$ or 1.8π, as can be seen from Fig. 2(a), for $b = 1.8$ the number of particles changes from a 10^8 at $\psi = 1.3\pi$ [see Fig. 2(b)] to nearly zero at $\psi = 1.8\pi$ (data not shown in figures). This indicates that the results of the simulations are quite sensitive to b and ψ, so that the curve found in Fig. 2(a) for the injection phase dependence at injection amplitudes of 2.0 is not readily applicable to other values of this parameter.

The value of $\psi = 1.3\pi$ is used for the simulations of Fig. 2(b) since it seems to be close to an optimal injection phase, judging from the data of Fig. 2(a). As a function of the injection amplitude, the normalized emittance and the energy spread do not seem to show any systematic behavior on the scale that is resolved by the simulations. The values of the energy spread vary between 4% and 18%, while the values for the emittance are between 10π and 40π mm mrad. Depending on the application, these variations will place a limit on the tolerable shot to shot laser jitter.

The number of trapped electrons, on the other hand, seems to show a systematic behavior. What should be expected is that the number of trapped particles first rises with increasing injection amplitude and then falls off. This is recognizable in the figure, even though the curve is quite noisy. The decrease with an increased amplitude causes an increase in transverse momentum, P_2, that is transferred to the particles by the injection pulse. At a certain value, the transverse momentum becomes large enough to prevent the trapping of the particles.

We may use Fig. 2(a) and Eqs. (13) and (14) to obtain an interesting scaling law for the brightness of the plasma cathode injector. The normalized brightness can be defined by $B_n = I/\varepsilon_n^2$ [16] for axially symmetric beams. For the average current of a bunch, we find $I \propto N/T_p = N\omega_p$, where T_p is the plasma wave period. As noted earlier, N scales with $n^{-1/2}$, while ω_p scales as $n^{1/2}$. Therefore, the product $N\omega_p$ does not depend on the density as the simulation results are scaled to different densities for fixed values of ω_0/ω_p, a, and b. For example, at $\psi = 1.8\pi$, we obtain $I_{\max} = 220$ A and $\varepsilon_n = 11\pi$ mm mrad $[(10^{16}\ \text{cm}^{-3})/n]^{1/2}$ which scales as $n^{-1/2}$. Combining these results predicts a brightness of $B_n = 1.8 \times 10^7 n/(10^{16}\ \text{cm}^{-3})$A/cm^2, which scales linearly with density.

The insensitivity of the beam current to the plasma density should also hold if ω_p, a, and b are changed. This can be argued as follows. The beam current can be written as $I = e n_b c \sigma^2 \pi$, where n_b is the beam density. If we normalize n_b with respect to the plasma density n_0 and the spot size σ with respect to c/ω_p, we find that

$$I = e n_0 c (\pi c^2/\omega_p^2) \frac{n_b}{n_0} (\sigma c/\omega_p)^2 = \frac{I_A}{4} \frac{n_b}{n_0} (\sigma c/\omega_p)^2. \tag{15}$$

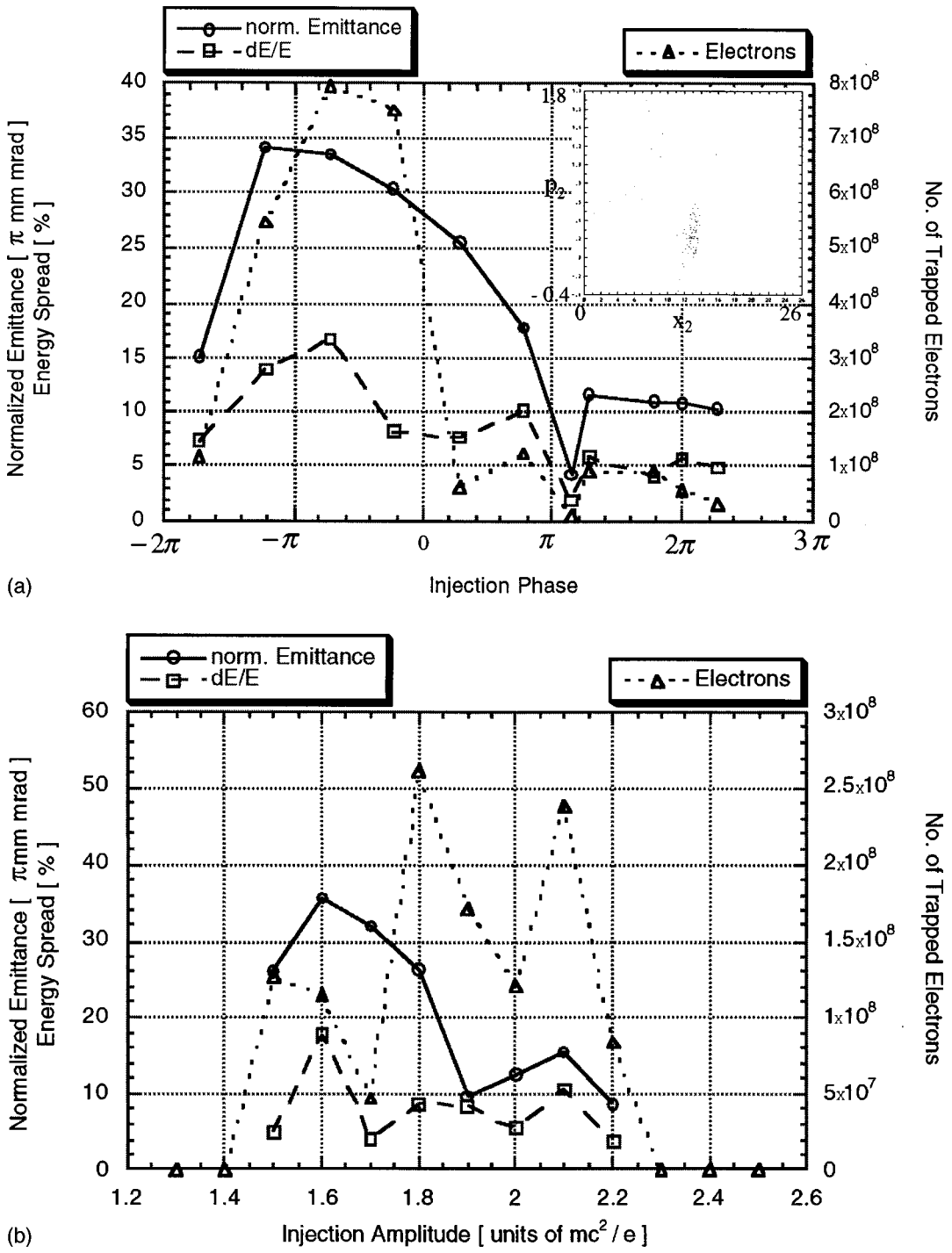

FIG. 2. (a) The number of trapped electrons, the normalized emittance, and the energy of the trapped particles as a function of the injection phase. The injection amplitude b is 2.0, and the drive amplitude a is 1.0. The connecting lines between the data points have been added to make it easier to distinguish the different data. The inset shows the raw data for the transverse phase space of the trapped particles that is used to calculated the emittance for the simulation at $\psi = 1.8\pi$. (b) The number of trapped electrons, the normalized emittance, and the energy spread of the trapped particles as a function of the injection amplitude. The injection phase ψ is 1.3π. All other parameters are the same as the ones used in the simulations of (a). The connecting lines between the data points have been added to make it easier to distinguish the different data.

This expression for I is insensitive to the plasma density for various laser parameters, if the normalized beam density and the spot size are relatively insensitive to the plasma density. We expect that the ratio n_b/n_0 is not a strongly varying function of $\gamma_\phi = \omega_0/\omega_p$, since the trapping threshold asymptotes for large γ_ϕ [see Eq. (4)]. Note also that since n_b/n_0 is typically less than 1 and σ is typically c/ω_p or less, this shows that the current is typically some fraction of the Alfven current.

It is interesting that despite their high brightness and density, the bunches are not space charge dominated. From the discussion above, I/I_A is of the order of 10^{-2}, while $(\sigma/\varepsilon_n)^2$

is typically of order unity. Thus, using Eq. (8), we find that $\rho \ll 1$ at all times in the plasma, and the beam is emittance dominated. We note that once the bunch leaves the plasma and expands in free space, it can rapidly become space charge dominated. For beams generated by the cathodeless injection scheme, this typically occurs in a distance of the order of $1\ \mathrm{cm} \times [(10^{16}\ \mathrm{cm}^{-3})/n]^{1/2}$. Since the effects of space charge can be neglected, it is possible to apply Eq. (9), the condition for matched beams. For the simulation parameters, the left side of Eq. (9) has values between 2 and 3, which means the external force term is larger than the diffraction term. For the beam emittances in the simulations, we also note that ε_n is between 0.01 and 0.12 times the plasma wave acceptance that was calculated above. The numbers for the matched beam condition and the emittance to acceptance ratio indicate that once the electrons are ''injected'' they are well within the parameters of stable acceleration for the plasma wave.

To achieve high energies in the LWFA the laser pulse must propagate through many diffraction or Rayleigh lengths of plasma. One way to guide a pulse is to use a parabolic density channel [19,20]. Therefore the cathodeless injection scheme may need to work in plasma channels. We have carried out a simulation in which the drive pulse propagated down a channel and the injection pulse propagated across the channel. The channel had a width of $3.25c/\omega_p$ and the density was decreased by 40% in the middle of the channel. In the simulation the number of trapped particles as well as the emittance of the particle bunch are reduced to about 20% from their values in the uniform plasma case. We also note that in all results presented in this paper the plasma is cold. We have done simulations with a 1-KeV plasma, and the number of electrons as well as the emittance decrease to about 40% of the cold plasma values.

Insight into the mechanism of trapping can be gained by studying the original location and trajectories of the trapped particles. In Fig. 3, we plot the original (x_1, x_2) positions for all the trapped particles from two simulations. The red points are for $\psi = 1.8\pi$ and $b = 2.0$, while the blue points are for a $\psi = 1.3\pi$ and $b = 1.8$. There are several important points to be noted. The first is that for both cases the particles are to the left of the injection pulse. Therefore, these particles experience a transverse ponderomotive force to the left not to the right, as was presumed in Ref. [1]. We have verified this by rerunning the simulations without the drive pulse to see only the effect of the injection pulse.

To gain a deeper understanding of the process, we follow the momentum of a single, typical, trapped particle as function of time in the 2D simulation. We consider a particle for the case of $\psi = 1.3\pi$ and $b = 1.8$. The data are shown in Fig. 4(a). The initial momentum is zero, since the simulation uses cold plasma. Here we show the results for only one particle, but the curves are very similar for other trapped particle phase space trajectories in this simulation.

The solid curve in Fig. 4(a) shows the longitudinal momentum of the particle; the dotted curve shows p_1 for the same particle in a simulation where the injection pulse is not launched. As expected, the same particle simply oscillates in the wake of the drive pulse. In the full simulation, we can see that the injection pulse has completely passed by the test particle at about the time $t = 31.7$. Although the injection pulse has an impact on the particle, the really large changes occur later at a time when the injection pulse has already left the area of the test particle. This indicates that the trapped particle receives the extra momentum needed for becoming trapped from the interaction of the two plasma wake fields created by these pulses, rather than from any effect directly related to the laser pulses (since those have already left the area of the particle). Note that the trapped particle goes through one full oscillation (accelerating, decelerating, and accelerating again) before it is trapped. This feature, that the particles become trapped in a multistep process (acceleration-deceleration-acceleration) caused by the interaction of the wake fields, is not unique to this particular simulation. Other simulations with different values for ψ and b showed the same process.

Figure 4(b) shows the E_1 field at $t = 42.0$. The blue areas accelerate, while the red areas decelerate electrons with respect to the x_1 direction. The green cross marks the position of the test particle shown in Fig. 4(a) at that time. The position of the particle in this picture is consistent with the development of p_1 in Fig. 4(a). The particle is at the edge of the accelerating area, and will slip back into the decelerating area. The field magnitude of the decelerating area is clearly smaller than that of the accelerating area. The spatial structure of the E_1 field seen in this figure can qualitatively be understood as mainly a superposition of the longitudinal field of the drive pulse wake and the transverse field of the injection pulse wake.

The question that arises at this point is whether this effect is mostly a linear effect that arises from the superposition of the two plasma waves, or whether it is essentially a nonlinear effect arising from the interaction of the two plasma waves mediated by the plasma. To address this question, we show the results of non-self-consistent 2D simulations and 1D numerical calculations (Fig. 5). The 2Df non-self-consistent simulations are done by turning off the field solver of the PEGASUS code, and instead calculating the fields of the lasers and their wakes analytically from linear theory at each time step [15]. As a result, it is possible to follow test particles in the fields caused by the linear superposition of the two laser pulses and their wakes. In a second non-self-consistent 2D simulation, the injection pulse is neglected while the linear wake it produces is not.

The 1D numerical calculations use the following electric fields for the wakes to calculate the trajectory of a particle:

Wake from the drive pulse:

$$E_D = E_{D,\max} \sin(k_p x - \omega_p t - \varphi_0). \tag{16}$$

Wake from the injection pulse:

$$E_I = E_{I,\max} 2e^{1/2} \sin(\omega_p t) x/w_0 e^{-2(x/w_0)^2}. \tag{17}$$

These equations follow from the ones used for the non-self-consistent 2D simulations. The laser fields are also omitted in this 1D calculation. The initial conditions of the particle are given by its position in the plasma wave described by Eq. (16). $E_{D,\max}$ and $E_{l,\max}$ are taken as 0.45 and 0.35, since these are the values seen in the self-consistent calculation with $\psi = 1.3\pi$ and $b = 1.8$. For the 2D non-self-consistent simulations, the laser amplitudes are slightly adjusted to yield those values, too. All other parameters of the non-self-

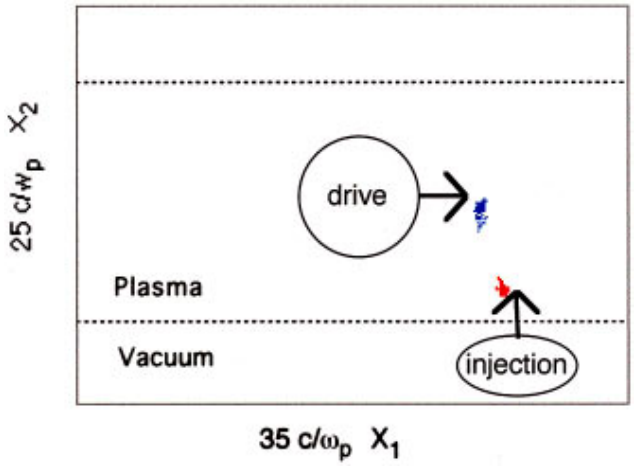

FIG. 3. (Color). The figure shows the initial position of trapped particles for two different simulations. The red particles come from a simulation with $\psi=1.8$ and $b=2.0$. The blue particles come from a simulation with $\psi=1.3$ and $b=1.8$. The position of the drive pulse in the figure is illustrative and does not match $\psi=1.3$ or $\psi=1.8$.

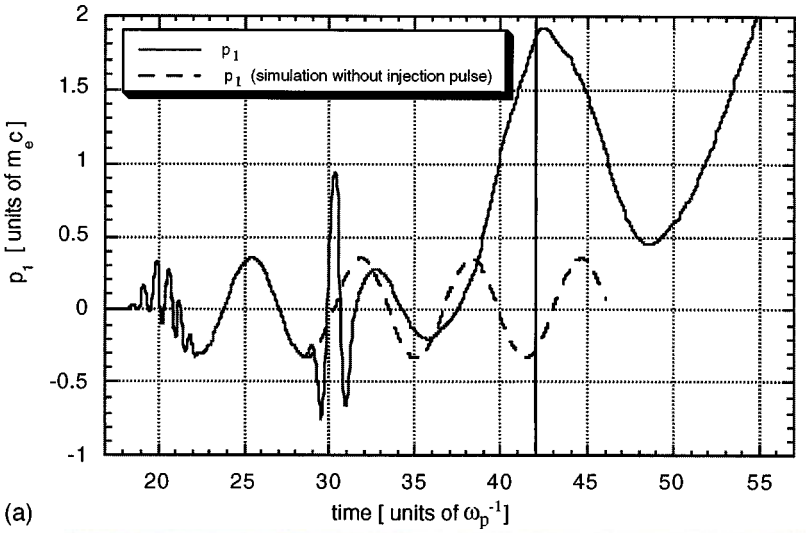

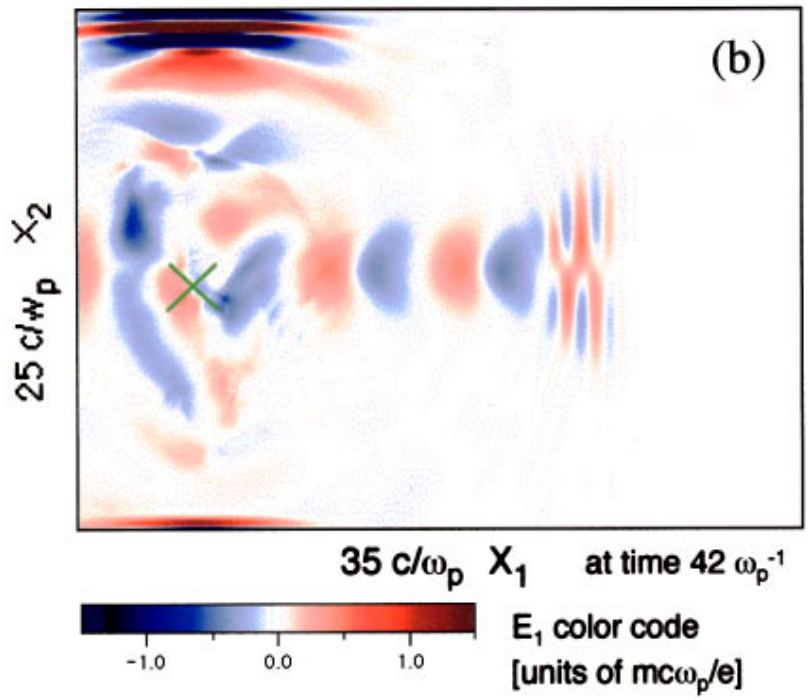

FIG. 4. (a) p_1 of a test particle as a function of time. The two curves are the results from simulations with (solid) and without (dashed) an injection pulse. $\psi=1.3\pi$ and $b=1.8$ for the simulation with an injection pulse. The initial position of the test particle is given by offsets of -2.3 in x_1 and -0.1 in x_2 relative to the intersection of the pulses (see Fig. 3). The vertical line in the figure indicates the time $t=42.0$ at which the electric fields are given in (b). (b) (Color). The field E_1 field at the time $t=42.0$ for $\psi=1.3$ and $b=1.8$. The cross indicates the position of the test particle shown in (a).

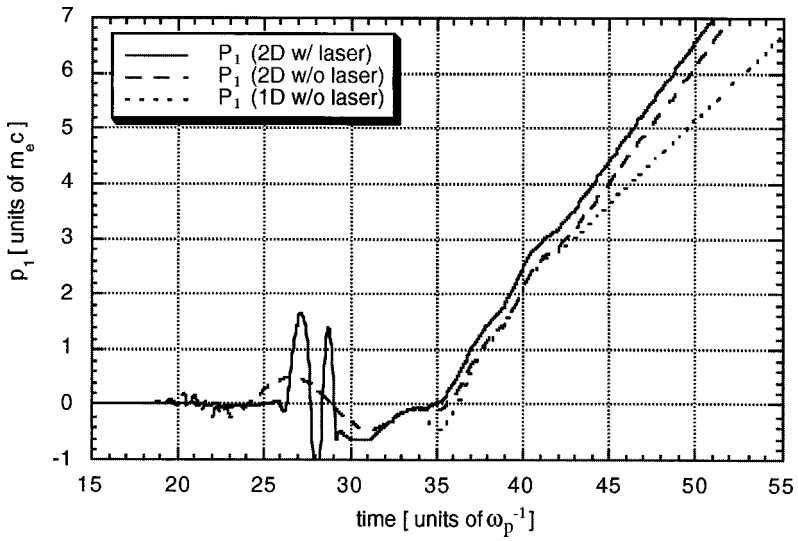

FIG. 5. p_1 vs time for a particle in a 2D non-self-consistent simulation (solid/dashed) and for a 1D numerical calculation (dotted). The 1D calculation had the starting parameters $x_0=-0.5$, $w_0=-1.5$, and $\varphi_0=\frac{4}{3}\pi$.

consistent 2D simulations and the 1D calculations are the same as in the self-consistent simulation with $\psi=1.3\pi$ and $b=1.8$, unless stated otherwise.

The results of these idealized models can be seen in Fig. 5. The linear superposition of two crossed plasma waves (solid line) creates conditions under which particles get trapped. On the other hand, the actual development of p_1 after the injection pulse has passed the particle looks different from the self-consistent results, which suggests that the trapping process is modified by the nonlinear interaction between the two plasma waves. The multistep trapping discussed above seems to be a result of this modification.

The result of the 2D simulation without the injection laser (dashed line) differs strongly from the one with the laser up to time the injection pulse has passed. After that time the two curves are rather similar, and they differ mainly due to a small displacement of one compared to the other along the time axis. Noting that the two curves belong to particles with a different original position in the simulation suggests that the effect of the ponderomotive force is to change which particles are trapped. Direct comparison of the temporal evolution between the 1D and 2D results is complicated, because the same particles are not trapped. We place the 1D curve in such a way that it is easy to compare the trajectories once a particle is trapped. The similarity of this curve with the curves from the non-self-consistent 2D simulations indicates that the basic physics of the trapping can be studied by Eqs. (16) and (17).

We close this section by commenting that determining whether the trapping results from a ponderomotive kick or from interfering wakes is important to developing simplified models to explain and extend the scheme investigated here. Our results suggest that the trapping is due to the interaction of two plasma waves rather than a plasma wave and a ponderomotive kick (impulse). However, this does not rule out the possibility that a different choice of parameters for the injection pulse will result in trapping due to a direct kick by the transverse ponderomotive force [21]. A possible advantage of the mechanism found in this paper relates to Eq. (15). If the trapping of particles is caused by dephasing them with respect to the accelerating wake, as we find it here, rather than from directly increasing their momentum, then n_b/n_0 could be a much weaker function of $\gamma_\phi=\omega_0/\omega_p$, indicating that this injection method might also be useful for larger γ_ϕ.

Understanding the trapping mechanism allows one to propose and understand other possible geometries. A copropagating geometry is the easiest to visualize [21]. The second pulse should be tightly focused to interact with a single bucket (or perhaps a few buckets), and it should be phased to enhance the original wake to amplitudes above wave breaking. In this geometry, the ponderomotive force and the wake are intimately connected for the first oscillation. However, in subsequent oscillations the interaction of the wakes could lead to injection. In simulations of this scheme we have observed an additional trapping mechanism at the plasma boundary. This mechanism might be of interest for experiments in which the plasma boundaries are sharp.

A counterpropagating geometry is more complicated. (This scheme differs from a recent idea of Esarey *et al.* [22], which considered a colinear geometry with an intense pump pulse and two counterstreaming injection pulses). Once again a second pulse is focused tightly to interact with only a single bucket. In this case the injection pulse is phased to reinforce the electrons motion as they move backwards. Therefore, the wake is unequivocally essential in order for the electrons to be trapped as they oscillate forward.

In another possible scenario, a plasma wave moving across the first wake (other geometries are also possible) could be gradually built up over time until a trapping threshold is reached. This scheme also clearly would rely only on the interfering wakes.

CONCLUSIONS

In this paper, using 2D PIC computer simulations, we studied the injection scheme recently proposed in Ref. [1]. We find that the beam brightness and quality compares rea-

sonably with that of electron bunches produced using conventional technologies. However, we find that the mechanism for the trapping of particles is not the transverse ponderomotive force of the injection pulse, but rather the interaction of the particles with the two plasma wakes.

These results open up a number of possibilities for future investigations, both to obtain analytical models and to consider other injection schemes and geometries. One important goal of future research would be to find an analytical model of the process that is able to predict the results seen in the simulations. This could then be used to determine fundamental limits on beam number and emittance, as well as to optimize parameters to achieve these limits. Another research direction is to use higher resolution 2D simulations, and to use 3D PIC simulations with more realistic laser parameters.

ACKNOWLEDGMENTS

We acknowledge useful conversations with E. Dodd, and Dr. E. Esarey, Dr. C. Joshi, and Dr. D. Umstadter. The work was supported by DOE Grant No. DE-FG03-92ER40727, LLNL Contract Nos. B291465 and B335241, and NSF Grant No. DMS-9722121. This work was performed under the auspices of the U.S. Department of Energy by Lawrence Livermore National Laboratory under Contract No. W07405-Eng-48.

[1] D. Umstadter, J. K. Kim, and E. Dodd, Phys. Rev. Lett. **76**, 2073 (1996).
[2] A. Ogata, IEEE Trans. Plasma Sci. **24**, 453 (1996).
[3] T. Tajima and J. M. Dawson, Phys. Rev. Lett. **43**, 267 (1979).
[4] C. Joshi *et al.*, Nature (London) **311**, 525 (1984).
[5] P. Chen *et al.*, Phys. Rev. Lett. **54**, 693 (1985).
[6] E. Esarey *et al.*, IEEE Trans. Plasma Sci. **24**, 252 (1996) and references therein.
[7] J. S. Fraser and R. L. Sheffield, IEEE J. Quantum Electron. **QE-23**, 1489 (1987).
[8] R. Williams *et al.*, Laser Part. Beams **8**, 427 (1990); T. Katsouleâs *et al.*, in *Laser Acceleration of Particles*, edited by C. Joshi and T. Katsouleas, AIP Conf. Proc. No. 130 (AIP, New York, 1985).
[9] R. Fedele *et al.*, Phys. Rev. A **33**, 4412 (1986).
[10] P. Mora, Phys. Fluids B **4**, 1630 (1992); J. Appl. Phys. **71**, 2087 (1992).
[11] E. Esarey and M. Pilloff, Phys. Plasmas **2**, 1432 (1995).
[12] L. M. Gorbunov *et al.*, Phys. Rev. Lett. **76**, 2495 (1996).
[13] W. B. Mori, Bull. Am. Phys. Soc. **32**, 1799 (1987); the total dc focusing force is 3/2 times larger than that given in Ref. [12], because of an additional electrostatic field.
[14] J. D. Lawson, *The Physics of Charged Particle Beams*, 2nd ed. (Oxford University Press, New York, 1988).
[15] P. Sprangle, E. Esarey, A. Ting, and G. Joyce, Appl. Phys. Lett. **53**, 2146 (1988).
[16] M. Reiser, *Theory and Design of Charged Particle Beams* (Wiley, New York, 1994).
[17] K. C. Tzeng, W. B. Mori, and C. D. Decker, Phys. Rev. Lett. **76**, 3332 (1996); PEGASUS uses the current deposition scheme in ISIS.
[18] T. Katsouleas *et al.*, Part. Accel. **22**, 81 (1987).
[19] P. Sprangle *et al.*, Phys. Rev. Lett. **69**, 2200 (1992).
[20] C. G. Durfee III and H. M. Milchberg, Phys. Rev. Lett. **71**, 2409 (1993).
[21] D. Umstadter (private communication); Bull. Am. Phys. Soc. **42**, 1184 (1997).
[22] E. Esarey *et al.*, Phys. Rev. Lett. **79**, 2682 (1997).